Localized Surface Plasmon Resonance in Lithographically Fabricated Single Gold Nanowires

ARTICLE *in* THE JOURNAL OF PHYSICAL CHEMISTRY C · MAY 2010

Impact Factor: 4.77 · DOI: 10.1021/jp1014725

3 AUTHORS, INCLUDING:

Heh-Nan Lin
National Tsing Hua University
42 PUBLICATIONS **693** CITATIONS

Localized Surface Plasmon Resonance in Lithographically Fabricated Single Gold Nanowires

Hsiang-An Chen, Hsin-Yu Lin, and Heh-Nan Lin*

Department of Materials Science and Engineering, National Tsing Hua University, Hsinchu 30013, Taiwan

Received: February 17, 2010; Revised Manuscript Received: May 4, 2010

We report a study of localized surface plasmon resonance (LSPR) in single Au nanowires (NWs) created by atomic force microscopy nanolithography with widths and thicknesses of less than 110 and 30 nm, respectively, and lengths of a few micrometers. Two LSPR peaks at around 630 and 490 nm in wavelength are observed, and the intensity is strongest when the incident electric field is parallel to the length direction of a NW. The polarization dependence is due to the lack of well-defined axes in the cross section of a NW from transmission electron microscopy analysis. The current results are in strong contrast to previous results of lithographically fabricated NWs, in which a single resonance mode is observed and corresponds to electron oscillation along the width direction. The present work reveals the interesting variation of LSPR modes in single metal NWs that are potentially valuable for future plasmonic applications.

1. Introduction

In recent years, noble metal nanostructures have attracted increasing interests in the development of sensitive biosensors and novel photonic devices due to their pronounced optical properties related to surface plasmons (SPs), which are the collective oscillations of conduction electrons at a metal−dielectric interface.[1–3] If all three geometric dimensions of a metal nanostructure are smaller than the SP wavelength, the plasmons are localized. On the other hand, the SPs are able to propagate if one dimension or more of the metal nanostructure is larger than the plasmon wavelength. The propagating SPs are usually called surface plasmon polaritons.[3]

When localized SPs are generated in a metal nanostructure, the electromagnetic field near the surface of the metal is enhanced. If the metal nanostructure is illuminated by a white-light source, specific optical scattering (i.e., Rayleigh scattering or elastic scattering), absorption, and extinction properties can be found in the corresponding spectra, and the peaks in the spectra are usually called localized surface plasmon resonance (LSPR) peaks.[1,2] The LSPR properties in a variety of metal nanostructures have been investigated extensively, including nanoparticles (NPs),[1,4,5] nanorods,[6–8] nanoplates,[9] nanorings,[10,11] nanotriangles,[12] and so forth. The well-known Mie theory[1,2] is the exact analytical solution for light scattering by spherical particles in an isotropic medium and explains the LSPR peaks in metal NPs with great success. The LSPR characteristics depend on the metal dielectric constant, size, and shape[2,13–15] and the dielectric constant of the surrounding medium.[16–18] In addition, the polarization of the incident light has also been found to affect the LSPR behavior in metal nanowires (NWs).[19–21] Because of the strong field enhancement effect at resonance, various applications, including as SP resonance biosensors,[8] surface-enhanced Raman scattering,[4,5,22] and other surface-enhanced spectroscopy,[23] have been reported.

Although there are some reported studies on metal NWs, they are less explored and not so well-understood as metal NPs. In addition, a metal NW with its cross section much smaller and length much larger than the SP wavelength is able to support both localized and propagating SPs. Therefore, it is worth while to understand more plasmonic properties of metal NWs. In this work, a white-light optical scattering technique is utilized to study LSPR in single Au NWs that are fabricated by a combination of atomic force microscopy (AFM) nanolithography[24] on a thin film resist, metal deposition, and lift-off. The NWs have widths and thicknesses of less than 110 and 30 nm, respectively, and lengths of a few micrometers. Two LSPR modes have been found with peak wavelengths at around 630 (red) and 490 (blue) nm. The blue mode has been not observed in other lithographically prepared Au NWs.[20,21] In addition, the observed polarization dependence is in strong contrast to previous studies.[20,21] The present work reveals the interesting variation of LSPR modes in a single NW due to different fabrication techniques.

2. Experimental Section

Fabrication and Characterization of Au NWs. A solution of 1 wt % poly(methylmethacrylate) (PMMA) in chlorobenzene was prepared and spin-coated onto a Si substrate with a 1 μm thick thermal oxide layer. The substrate was baked at 150 °C for 30 min, and a thin PMMA film with a thickness of 50 nm was formed. A commercial AFM (Smena-B, NT-MDT) and a rectangular Si probe (NSC15, MikroMasch) were employed for creating a nanogroove on the PMMA film by nanoscratching. A 1 nm thick Ti film (as an adhesion layer) and a Au film with a thickness ranging between 7 and 30 nm were deposited in sequence onto the substrate by e-beam evaporation. The PMMA film was then removed in acetone in an ultrasonic bath. The sample was finally dried by nitrogen gas, and a Au NW was fabricated. A NW array could also be created by the same procedure with multiple nanoscratchings. Details of the fabrication procedure can be found in our previous publications.[25,26] The thicknesses of the fabricated NWs were determined by the AFM and the widths by a field emission scanning electron microscope (SEM, JSM 6500F, JEOL). The cross-sectional shapes of the NWs were characterized by a transmission electron microscope (TEM, JEM 2010, JEOL). Incidentally, a Au nanodot (ND) array was fabricated in a similar fashion by

* To whom correspondence should be addressed. E-mail: hnlin@mx.nthu.edu.tw.

10.1021/jp1014725
Published on Web 05/20/2010

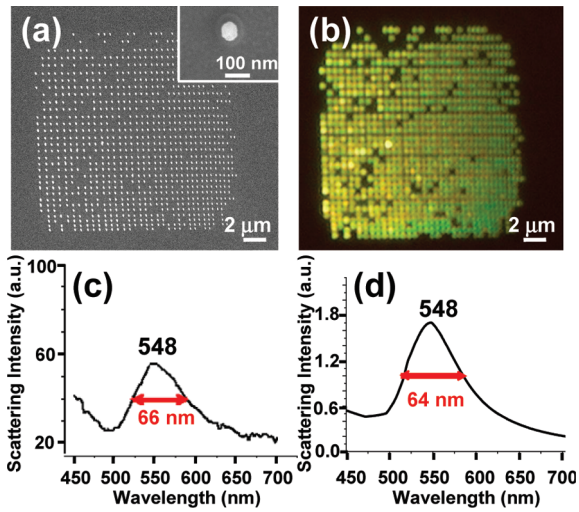

Figure 1. (a) The SEM image of a Au ND array and (b) the corresponding dark-field optical image. The inset in (a) is an enlarged view of a ND with a diameter of around 72 nm. (c) The scattering spectrum of the ND array and (d) the numerically calculated scattering spectrum of a Au ND with a diameter of 72 nm in a homogeneous medium with a refractive index of 1.25 based on the Mie theory. Both spectra have a resonance peak at 548 nm.

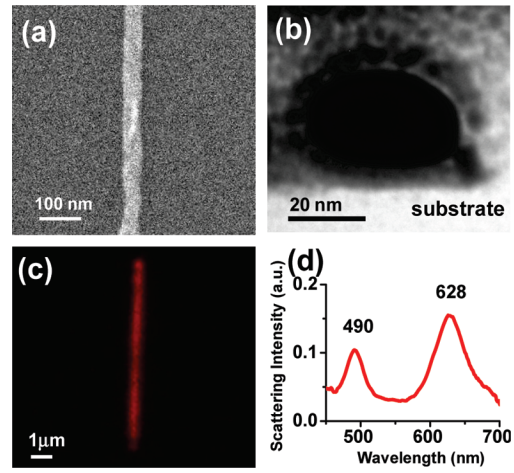

Figure 2. (a) The SEM and (b) the TEM images of a fabricated single Au NW and its cross section, respectively. (c) The dark-field optical image of a Au NW with a width and a thickness of 70 and 22 nm, respectively, and (d) the corresponding scattering spectrum that shows two LSPR peaks at 490 and 628 nm.

nanoindenting. The nanodots were originally disklike but became spherical after being annealed at 900 °C for 30 min. The array was used for testing the white-light scattering spectrum measurement system.

White-Light Scattering Measurement. The scattering spectrum of a single Au NW on a Si substrate was measured in the dark-field mode by using an optical microscope (BX51, Olympus) with a 100 W halogen white-light source (with a removable polarizer in front) and a 100× objective lens (numerical aperture = 0.9). (A schematic diagram is provided in the Supporting Information.) At this high magnification, the position of the NW could be located precisely, and it facilitated the confirmation of the detected light from the NW. Also, the NW was placed on a rotational stage, and the angle between the NW and a polarized light beam could be controlled. The scattered light went through the optical path in the microscope and was focused into an optical fiber. A second polarizer was placed in front of the fiber when polarized detection was needed. The fiber was connected to a spectrometer (BRC111A, BWTek) and the spectrum was obtained. The error of the spectrometer was around 0.5 nm in wavelength.

3. Results and Discussion

To verify if the optical scattering spectrum measurement setup was working normally, a Au ND array was fabricated on a Si substrate (with a thick thermal oxide layer) first for testing. The SEM image of the ND array is shown in Figure 1a, and the NDs have a spherical shape with an average diameter of around 72 nm, as can be seen in the inset. The dark-field image is shown in Figure 1b, and it appears green. The LSPR spectrum of spherical Au NDs can be described by the Mie theory and calculated numerically.[27] The experimental scattering and the calculated spectra are shown in Figure 1c,d, respectively, and both have a peak at 548 nm. The calculated spectrum was obtained with the use of a medium refractive index of 1.25, which is the average refractive index of air and quartz. The use of an average refractive index of the upper medium and the substrate for the homogeneous surrounding medium in the calculation of the Mie theory has been previously found an effective approach for substrate-supported spherical NDs.[28] Furthermore, the difference between the half-widths of the two spectra is only about 3%. The consistency between the experimental and the calculated scattering spectra assures the correct functionality of the scattering spectrum measurement setup.

The SEM and the TEM images of a fabricated single Au NW and its cross section are shown in Figure 2a,b, respectively. The cross-sectional shape is similar to an ellipse but with less convex sides. (The cross section of another NW is provided in the Supporting Information). The curved shape at the bottom of the NW was caused by the AFM tip apex, which had a diameter of around 20 nm or larger. The curved shape at the top, on the other hand, was caused by the pile-up of PMMA on both sides of the nanogroove, which was created after nanoscratching,[26] which subsequently reduced the amount of evaporated metal on the sides. The dark-field optical image of a different NW with a width and a thickness of 70 and 22 nm, respectively, is shown in Figure 2c and appears reddish. The scattering spectrum of the NW is shown in Figure 2d and is composed of two LSPR peaks at 490 and 628 nm in the blue and the red optical regions, which suggests the occurrence of two resonance modes.[14,29] The lack of well-defined axes in the cross section, as shown in Figure 2b, has significant influence on the polarization of the LSPR modes and will be discussed later.

The AFM tip was then used to cut a NW to investigate the influence of the length on the two resonance peaks. A NW was first cut at the middle, and two separate NWs were generated. The two NWs were further cut at the middle, and four separate NWs were finally created. Therefore, all the NWs had the same width and thickness but with different lengths. Furthermore, the gaps between the NWs were made larger than 200 nm, and the coupling between adjacent NWs was negligible.[30] Three scattering spectra were taken, and they correlated with the original NW, the two NWs after the first cut, and the final four NWs. The SEM image of such an example of the final four NWs with a width of 110 nm and a thickness of 20 nm and the correlated scattering spectra are presented in Figure 3a,b, respectively. (It should be noted that the SEM image was taken at the last stage because it was found that the scattering intensity of a NW increased after SEM imaging.) As can be seen in Figure 3b, the scattering spectra are almost identical even though the final

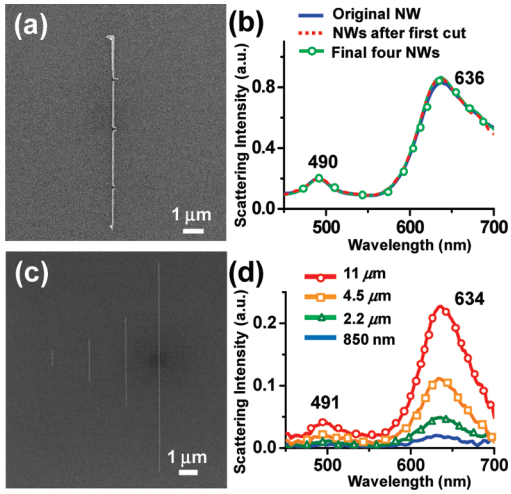

Figure 3. (a) The SEM image of four Au NWs with a width of 110 nm and a thickness of 20 nm created by three cuttings. (b) Scattering spectra of the original NW, the two NWs after the first cut at the middle, and the final four NWs. (c) The SEM image of four different NWs with the same width and thickness and (d) the corresponding scattering spectra.

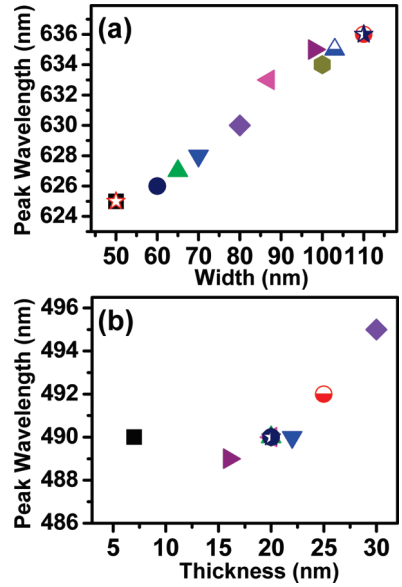

Figure 4. (a) A plot of the red LSPR peak wavelength versus the NW width. (b) A plot of the blue LSPR peak wavelength versus the NW thickness. The wavelength error for both peaks is around 1 nm. The data points are from 12 different NWs, and the two peaks from the same NW are marked with the same symbol in (a) and (b).

NW length was only one-fourth of the original length. Another set of NWs with the same width and thickness but with different lengths down to 850 nm were also fabricated, and the SEM image is shown Figure 3c. The corresponding scattering spectra are shown in Figure 3d, and it is clear that the two peak wavelengths remain unchanged. All results indicate that the two LSPR peaks are insensitive to the NW length, at least down to the tested length of 850 nm.

To understand the influence of the width and the thickness of a NW on the LSPR peaks, 12 NWs with widths ranging between 50 and 110 nm and thicknesses ranging between 7 and 30 nm were fabricated and tested. The geometrical dimensions and peak wavelengths for the 12 NWs are tabulated in the Supporting Information. The uncertainty for the peak wavelength is around 1 nm. Although there can be four relationships between the two resonance peak wavelengths and the two NW geometrical dimensions, it turns out that only two relationships, namely, the red peak wavelength versus the width and the blue peak wavelength versus the thickness, appear rational and are shown in Figure 4a,b, respectively. The other two relationships are randomly varied and, therefore, not shown here. As can be seen in Figure 4a, the red peak experiences a linear red shift from 625 to 636 nm when the width is increased from 50 to 110 nm. On the other hand, the blue peak remains unchanged within the measurement error at around 490 nm when the thickness is below 22 nm and gradually shifts to 495 nm when the thickness is increased to 30 nm with a seemingly linear relationship, as shown in Figure 4b.

It is well-known that two LSPR modes due to electron oscillations along the major axis and the minor axis directions occur in a nanospheroid.[14,31] Therefore, it seems reasonable that the red peak is due to electron oscillation along the width direction and the blue peak due to oscillation along the thickness direction. Nevertheless, the interpretation raises ambiguity about the polarization of the scattered electric field. Considering the NW as a radiating dipole with a moment of **p** at the origin, the far-field electric field **E** can be expressed as[31]

$$\mathbf{E} = k^2 e^{ikr} \frac{\mathbf{r} \times (\mathbf{r} \times \mathbf{p})}{r^3}$$

where k is the wavenumber and **r** the position vector at the observation point. Because the observation point in the microscope is right above the NW, the electric field due to electron oscillation along the thickness direction and thus the blue resonance peak should not be observed. Indeed, the LSPR peak due to electron oscillation along the thickness direction in a substrate-supported NW has not been observed in previous reports.[20,21]

To clarify the polarization ambiguity, polarized illumination was first utilized. In the dark-field mode, a circular light stop was placed after the light source and a ring-shaped light (i.e., annular illumination) was approaching the objective lens and focused onto the NW sample. Nevertheless, it can be shown that the polarization of the focused light was actually not affected (see the Supporting Information). By rotating the sample stage, the dark-field optical images of a NW under parallel ($\alpha = 0°$) and perpendicular ($\alpha = 90°$) illuminations are shown in Figure 5a,b, respectively, where α is the angle between the polarization of the incident electric field and the length direction (the long axis) of the NW. As can be seen clearly, the scattering intensity under perpendicular illumination is much weaker. Seven scattering spectra of the NW were measured under polarized illumination with α varied from 0° to 90° at an interval of 15°, and the results are shown in Figure 5c along with the spectrum from unpolarized illumination. For polarized illumination, the scattering intensity is strongest when α is equal to 0°, but still less than that from unpolarized illumination as expected. The two LSPR peaks are also prominent, and the peak wavelengths are almost identical to those from the unpolarized spectrum. Nevertheless, the red peak is much sharper than that in the unpolarized curve. The scattering intensity decreases as the angle α increases and becomes weakest when α is equal to 90°, that is, when the electric field is perpendicular to the NW long axis. Although the resonance behavior is not obvious at this angle, two broad peaks do exist at similar spectral regions (see the Supporting Information).

The results shown in Figure 5c clearly reveal that the red or the blue LSPR mode cannot be regarded as electron oscillation along the width or the thickness direction, respectively, because

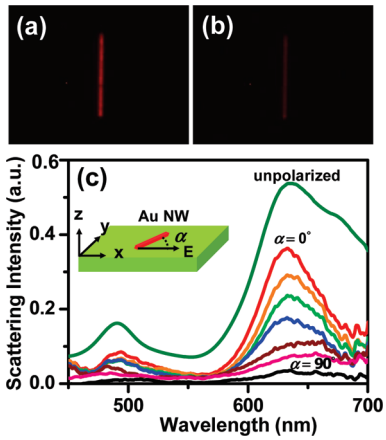

Figure 5. Dark-field optical images of a NW under (a) parallel ($\alpha = 0°$) and (b) perpendicular ($\alpha = 90°$) illuminations. (c) Scattering spectra of a Au NW under unpolarized and polarized illuminations. For the latter case, seven scattering spectra were measured by rotating the long axis of the NW relative to the incident electric field with the angle α varied from 0° to 90° at an interval of 15°.

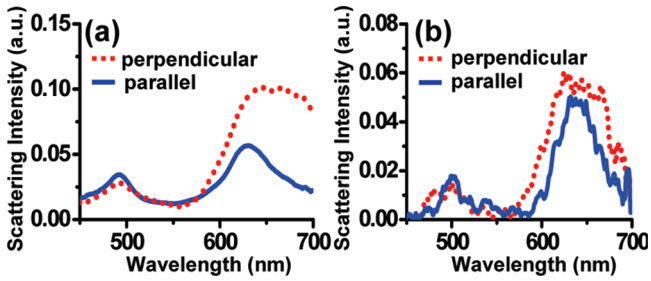

Figure 6. Scattering spectra of a single Au NW under (a) unpolarized and (b) parallel illuminations with polarized detection perpendicular (dotted line) and parallel (solid line) to the length direction of the NW.

the strongest scattering intensity occurs at $\alpha = 0°$ under polarized illumination. To further identify the polarization of the scattered light, a second polarizer was placed in front of the optical fiber and aligned parallel or perpendicular to the length direction of the NW. The resultant scattering spectra under unpolarized and parallel ($\alpha = 0°$) illuminations are shown in Figure 6a,b, respectively. Because of the weaker illumination intensity in the parallel polarization case, the spectra in Figure 6b are noisier. The perpendicular illumination was also tested, but the scattered light was rather weak (which is consistent with the 90° curve in Figure 5c), and the result is not shown.

In Figure 6b, the electric field of the scattered light has both parallel and perpendicular components even under parallel illumination. In addition, both LSPR modes are present in the parallel or the perpendicular spectrum. Because the blue mode is also dependent on the NW thickness (see Figure 4b), it is reasonable that the blue mode is related to combined electron oscillations along the length, the width, and the thickness directions in a NW. The red mode should also have this feature because the two modes are similarly excited. In other words, the radiating dipole moment of the NW for each LSPR mode has components along the three directions. The occurrence of the other two components (along the width and the height directions) under parallel illumination is presumably caused by the rearrangement of the electric field in the NW imposed by the boundary conditions. However, the two modes are still separately dependent on the width and the thickness, as has been shown in Figure 4.

The present observation of two LSPR modes and the obtained polarization dependence are in strong contrast to reported properties of LSPR modes in Au NWs prepared by other lithographic methods, and a comparison is provided in Table 1. As can be seen, only one resonance mode is observed in each Au NW with the peak wavelength in the red optical region in refs 20 and 21. In addition, the LSPR modes have been excited or observed perpendicularly (relative to the length direction) and attributed to electron oscillations along the width direction of the NWs. The variation in the polarization dependence is most likely caused by the cross-sectional shape produced by a fabrication technique. For example, the NWs in ref 21 have been created by nanoskiving and have a rectangular cross section. As a result, LSPR can be efficiently generated by a perpendicularly polarized incident electric field. On the other hand, the cross-sectional shape of our NWs (see Figure 2b) does not have a well-defined axis along the width direction, and the perpendicular excitation is, therefore, not efficient, although possible (see Figure 5c). Consequently, the radiating dipole field is stronger due to the much larger dipole moment induced under parallel excitation (because the NW length is much larger than its width) and shows the two LSPR modes. This argument also explains the observation of similar polarization dependence as ours in other reports. The LSPR modes induced by parallel illumination have been found in two reports of Ag NWs, which are also listed in Table 1, with the observation of broad peaks in the wavelength range between 500 and 700 nm instead of sharp peaks.[32,33]

Furthermore, the relationships between the peak wavelength and the geometrical dimensions are also different due to different cross-sectional shapes. A linear dependence between the peak wavelength and the height-to-width aspect ratio (and thus an inverse relationship between the wavelength and the width-to-height aspect ratio) has been well-established in ref 21. On the other hand, results of ours and ref 20 do not support such a linear dependence. It is also noticeable in Table 1 that the width-to-height aspect ratios are smaller than 1 in ref 21 but larger than 1 in ref 20 and the present work. All of these different properties reveal the interesting variation of LSPR modes due to different fabrication techniques.

In a metal nanostructure, the LSPR peak wavelengths in a scattering (or absorption or extinction) spectrum are affected by the shape and the size of the metal nanostructure, the metal dielectric property, and the refractive index of the surrounding medium.[13–18,31] Therefore, metal nanostructures can be used as chemical or biological sensors based on the LSPR peak shift due to chemical binding of a chemical or biological specimen onto the metal nanostructures.[1,2] To test the sensitivity of the fabricated single Au NWs, the scattering spectra before and after a PMMA thin film was deposited on the substrate with the NW were measured and are shown in Figure 7a. As the medium refractive index is changed from $n_{air} = 1$ to $n_{PMMA} = 1.5$, the red resonance peak wavelength of the NW (with a width of around 85 nm) shifts from 632 to 684 nm and represents a refractive index sensitivity of 104 nm R.I.U.$^{-1}$, which is equal to the wavelength shift divided by the refractive index change.[17,18,34] (It should be noted that the substrate refractive index is not considered in the calculation.) On the other hand, the blue resonance peak is rather weak after the deposition of PMMA, and it is difficult to determine the peak position. For comparison, the refractive index sensitivity of 50 nm long Au nanorods is around 170 nm R.I.U.$^{-1}$, as determined in a recent report.[35] Another test for the chemical sensing capability was also conducted by measuring the peak wavelength changes due

TABLE 1: Comparison of Substrates, Geometric Sizes, Resonance Peaks, and Polarization of LSPR in Au and Ag NWs in the Literature[b]

material	substrate	width (nm)	height (nm)	A. R.	peak (nm)	polarization[a]	reference
Au NW	glass	186	25	7.44	~740	perpendicular[a]	Kim et al.[20]
		206	47	4.38	~640		
		189	73	2.59	~620		
	silicon	10	30	0.33	~615	perpendicular[b]	Xu et al.[21]
		10	50	0.2	~650		
		20	50	0.4	~620		
		20	100	0.2	~720		
		40	70	0.57	~600		
		40	100	0.4	~630		
	silicon (with thick oxide)	50	7	7.14	625	parallel[a]	present work
		50	20	2.5	625		
		80	30	2.67	630		
		110	20	5.5	636		
		dia. (nm)					
Ag NW	silicon		~50		500−600 nm (a broad peak)	parallel[a] and perpendicular[a]	Tao et al.[32]
	silicon		~100		500−700 nm (a broad peak)	parallel[a]	Du et al.[33]

[a] Polarization in reference to the length direction (the long axis) of the NW. [a] denotes polarized illumination and unpolarized detection. [b] denotes unpolarized illumination and polarized detection. [b] Abbreviations: aspect ratio, A.R. (ratio of width to height); diameter, dia.

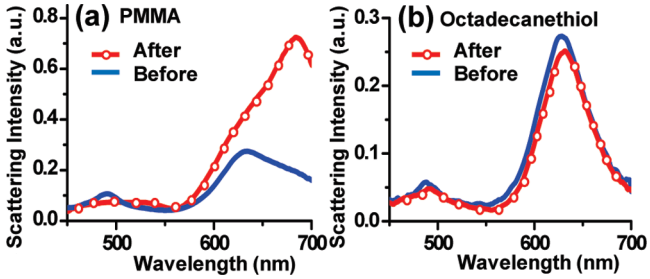

Figure 7. Scattering spectra of a Au NW before (solid curve) and after (dashed curve) the deposition of a PMMA film on the substrate. The red peak wavelength shifts from 632 to 684 nm. (b) Scattering spectra of a Au NW before and after the selective binding of an alkanethiolate self-assembled monolayer. The red peak wavelength shifts from 628 to 631 nm.

to the selective binding of an alkanethiolate self-assembled monolayer onto a Au NW.[36] A Au NW was immersed in a 20 mM octadecanethiol solution for 30 min and dried in air. A full coverage of the molecules on the NW was achieved.[36] The scattering spectra of the Au NW before and after the binding of the octadecanethiol molecules are shown in Figure 7b. The red peak shifts from 628 to 631 nm and the blue one from 489 to 491 nm. Although the wavelength shifts are not significant, they are larger than the 1 nm uncertainty and detectable.

4. Conclusions

In summary, LSPR in single Au NWs that are created by atomic force microscopy nanolithography has been investigated by a white-light optical scattering technique. The NWs have widths and thicknesses of less than 110 and 30 nm, respectively, and lengths of a few micrometers. In the scattering spectrum of a single NW, two localized surface plasmon resonance peaks exist at around 630 (red) and 490 (blue) nm in wavelength. The red and the blue resonance modes are found to be dependent on the width and the thickness, respectively, and a clear linear relationship is observed between the red peak wavelength and the NW width. The scattering intensity is strongest when the incident electric field is parallel to the length direction of the NW and weakest when perpendicular. Furthermore, the electric field of the scattered light has both parallel and perpendicular components even under parallel illumination. On the basis of these results, each LSPR mode should be related to combined electron oscillations with components along the length, the width, and the thickness directions in a NW.

The present observation of two LSPR modes and the obtained polarization dependence are in strong contrast to previous results of lithographically fabricated Au NWs, in which a single resonance mode is observed and corresponds to electron oscillation along the width direction. The variation in the polarization dependence is most likely caused by the cross-sectional shape produced by a fabrication technique. In the present work, the cross section of a NW is similar to an ellipse with less convex sides. The perpendicular excitation is not efficient due to the lack of well-defined axes in the cross section. Consequently, the radiating dipole field is stronger due to the much larger dipole moment induced under parallel excitation. Additionally, the fabricated Au NWs have a refractive index sensitivity of around 100 nm R.I.U.$^{-1}$ Chemical sensing of the binding of an alkanethiolate self-assembled monolayer onto a Au NW has also been achieved, and the peak wavelength change is around 3 nm. The present work reveals the interesting variation of LSPR modes in a single metal NW due to different fabrication techniques and provides a detailed polarization analysis that is potentially valuable for future applications of plasmonic metal NWs.

Acknowledgment. The authors acknowledge Yi-Jen Wu for technical assistance and Professors Din-Ping Tsai and Jia-Han Li at National Taiwan University for valuable discussions. This work was supported by the National Science Council under Grant Nos. 98-2120-M-002-004 (National Nanoscience and Nanotechnology Program) and 98-2112-M-007-022.

Supporting Information Available: A schematic diagram of the white-light scattering measurement setup, the SEM and the TEM images of another Au NW, the complete list of the geometrical dimensions and the peak wavelengths for the 12 NWs shown in Figure 4, the calculation of the incident electric field under annular illumination in the dark-field mode, and the enlarged curve of the $\alpha = 90°$ spectrum in Figure 5c. This material is available free of charge via the Internet at http://pubs.acs.org.

References and Notes

(1) Haes, A. J.; Stuart, D. A.; Nie, S. M.; Van Duyne, R. P. Using Solution-Phase Nanoparticles, Surface-Confined Nanoparticle Arrays and Single Nanoparticles as Biological Sensing Platforms. *J. Fluoresc.* **2004**, *14*, 355–367.

(2) Hutter, E.; Fendler, J. H. Exploitation of Localized Surface Plasmon Resonance. *Adv. Mater.* **2004**, *16*, 1685–1706.

(3) Pitarke, J. M.; Silkin, V. M.; Chulkov, E. V.; Echenique, P. M. Theory of Surface Plasmons and Surface-Plasmon Polaritons. *Rep. Prog. Phys.* **2007**, *70*, 1–87.

(4) Luo, W.; van der Veer, W.; Chu, P.; Mills, D. L.; Penner, R. M.; Hemminger, J. C. Polarization-Dependent Surface Enhanced Raman Scattering from Silver 1D Nanoparticle Arrays. *J. Phys. Chem. C* **2008**, *112*, 11609–11613.

(5) Yan, B.; Thubagere, A.; Premasiri, W. R.; Ziegler, L. D.; Dal Negro, L.; Reinhard, B. M. Engineered SERS Substrates with Multiscale Signal Enhancement: Nanoparticle Cluster Arrays. *ACS Nano* **2009**, *3*, 1190–1202.

(6) Mohamed, M. B.; Volkov, V.; Link, S.; El-Sayed, M. A. The 'Lightning' Gold Nanorods: Fluorescence Enhancement of over a Million Compared to the Gold Metal. *Chem. Phys. Lett.* **2000**, *317*, 517–523.

(7) Sieb, N. R.; Wu, N. C.; Majidi, E.; Kukreja, R.; Branda, N. R.; Gates, B. D. Hollow Metal Nanorods with Tunable Dimensions, Porosity, and Photonic Properties. *ACS Nano* **2009**, *3*, 1365–1372.

(8) Yu, C.; Irudayaraj, J. Quantitative Evaluation of Sensitivity and Selectivity of Multiplex NanoSPR Biosensor Assays. *Biophys. J.* **2007**, *93*, 3684–3692.

(9) Ye, J.; Chen, C.; Van Roy, W.; Van Dorpe, P.; Maes, G.; Borghs, G. The Fabrication and Optical Property of Silver Nanoplates with Different Thicknesses. *Nanotechnology* **2008**, *19*, 325702.

(10) Aizpurua, J.; Hanarp, P.; Sutherland, D. S.; Käll, M.; Bryant, G. W.; de Abajo, F. J. G. Optical Properties of Gold Nanorings. *Phys. Rev. Lett.* **2003**, *90*, 057401.

(11) Cleary, A.; Clark, A.; Glidle, A.; Cooper, J. M.; Cumming, D. Fabrication of Double Split Metallic Nanorings for Raman Sensing. *Microelectron. Eng.* **2009**, *86*, 1146–1149.

(12) Zhang, X. Y.; Hicks, E. M.; Zhao, J.; Schatz, G. C.; Van Duyne, R. P. Electrochemical Tuning of Silver Nanoparticles Fabricated by Nanosphere Lithography. *Nano Lett.* **2005**, *5*, 1503–1507.

(13) Grand, J.; de la Chapelle, M. L.; Bijeon, J.-L.; Adam, P.-M.; Vial, A.; Royer, P. Role of Localized Surface Plasmons in Surface-Enhanced Raman Scattering of Shape-Controlled Metallic Particles in Regular Arrays. *Phys. Rev. B* **2005**, *72*, 033407.

(14) Noguez, C. Surface Plasmons on Metal Nanoparticles: The Influence of Shape and Physical Environment. *J. Phys. Chem. C* **2007**, *111*, 3806–3819.

(15) Orendorff, C. J.; Sau, T. K.; Murphy, C. J. Shape-Dependent Plasmon-Resonant Gold Nanoparticles. *Small* **2006**, *2*, 636–639.

(16) Jensen, T. R.; Duval, M. L.; Kelly, K. L.; Lazarides, A. A.; Schatz, G. C.; Van Duyne, R. P. Nanosphere Lithography: Effect of the External Dielectric Medium on the Surface Plasmon Resonance Spectrum of a Periodic Array of Sliver Nanoparticles. *J. Phys. Chem. B* **1999**, *103*, 9846–9853.

(17) Tam, F.; Moran, C.; Halas, N. Geometrical Parameters Controlling Sensitivity of Nanoshell Plasmon Resonances to Changes in Dielectric Environment. *J. Phys. Chem. B* **2004**, *108*, 17290–17294.

(18) Miller, M. M.; Lazarides, A. A. Sensitivity of Metal Nanoparticle Surface Plasmon Resonance to the Dielectric Environment. *J. Phys. Chem. B* **2005**, *109*, 21556–21565.

(19) Staleva, H.; Skrabalak, S. E.; Carey, C. R.; Kosel, T.; Xia, Y. N.; Hartland, G. V. Coupling to Light, and Transport and Dissipation of Energy in Silver Nanowires. *Phys. Chem. Chem. Phys.* **2009**, *11*, 5889–5896.

(20) Kim, H. M.; Xiang, C. X.; Güell, A. G.; Penner, R. M.; Potma, E. O. Tunable Two-Photon Excited Luminescence in Single Gold Nanowires Fabricated by Lithographically Patterned Nanowire Electrodeposition. *J. Phys. Chem. C* **2008**, *112*, 12721–12727.

(21) Xu, Q. B.; Bao, J. M.; Capasso, F.; Whitesides, G. M. Surface Plasmon Resonances of Free-Standing Gold Nanowires Fabricated by Nanoskiving. *Angew. Chem.* **2006**, *118*, 3713–3717.

(22) Ko, H.; Singamaneni, S.; Tsukruk, V. V. Nanostructured Surfaces and Assemblies as SERS Media. *Small* **2008**, *4*, 1576–1599.

(23) Yonzon, C. R.; Stuart, D. A.; Zhang, X. Y.; McFarland, A. D.; Haynes, C. L.; Van Duyne, R. P. Towards Advanced Chemical and Biological Nanosensors—An Overview. *Talanta* **2005**, *67*, 438–448.

(24) Tseng, A. A.; Jou, S.; Notargiacommo, A.; Chen, T. P. Recent Developments in Tip-Based Nanofabrication and Its Roadmap. *J. Nanosci. Nanotechnol.* **2008**, *8*, 2167–2186.

(25) Hsu, J.-H.; Lin, C.-Y.; Lin, H.-N. Fabrication of Metallic Nanostructures by Atomic Force Microscopy Nanomachining and Lift-Off Process. *J. Vac. Sci. Technol., B* **2004**, *22*, 2768–2771.

(26) Chen, Y.-J.; Hsu, J.-H.; Lin, H.-N. Fabrication of Metal Nanowires by Atomic Force Microscopy Nanoscratching and Lift-Off Process. *Nanotechnology* **2005**, *16*, 1112–1115.

(27) Gopinath, A.; Boriskina, S. V.; Feng, N. N.; Reinhard, B. M.; Dal Negro, L. Photonic-Plasmonic Scattering Resonances in Deterministic Aperiodic Structures. *Nano Lett.* **2008**, *8*, 2423–2431.

(28) Curry, A.; Nusz, G.; Chilkoti, A.; Wax, A. Substrate Effect on Refractive Index Dependence of Plasmon Resonance for Individual Silver Nanoparticles Observed Using Darkfield Micro-Spectroscopy. *Opt. Express* **2005**, *13*, 2668–2677.

(29) Link, S.; Mohamed, M. B.; El-Sayed, M. A. Simulation of the Optical Absorption Spectra of Gold Nanorods as a Function of Their Aspect Ratio and the Effect of the Medium Dielectric Constant. *J. Phys. Chem. B* **1999**, *103*, 3073–3077.

(30) Jain, P. K.; Huang, W. Y.; El-Sayed, M. A. On the Universal Scaling Behavior of the Distance Decay of Plasmon Coupling in Metal Nanoparticle Pairs: A Plasmon Ruler Equation. *Nano Lett.* **2007**, *7*, 2080–2088.

(31) Kelly, K. L.; Coronado, E.; Zhao, L. L.; Schatz, G. C. The Optical Properties of Metal Nanoparticles: The Influence of Size, Shape, and Dielectric Environment. *J. Phys. Chem. B* **2003**, *107*, 668–677.

(32) Tao, A.; Kim, F.; Hess, C.; Goldberger, J.; He, R. R.; Sun, Y. G.; Xia, Y. N.; Yang, P. D. Langmuir—Blodgett Silver Nanowire Monolayers for Molecular Sensing Using Surface-Enhanced Raman Spectroscopy. *Nano Lett.* **2003**, *3*, 1229–1233.

(33) Du, C. L.; You, Y. M.; Kasim, J.; Ni, Z. H.; Yu, T.; Wong, C. P.; Fan, H. M.; Shen, Z. X. Confocal White Light Reflection Imaging for Characterization of Metal Nanostructures. *Opt. Commun.* **2008**, *281*, 5360–5363.

(34) Ni, W. H.; Chen, H. J.; Kou, X. S.; Yeung, M. H.; Wang, J. F. Optical Fiber-Excited Surface Plasmon Resonance Spectroscopy of Single and Ensemble Gold Nanorods. *J. Phys. Chem. C* **2008**, *112*, 8105–8109.

(35) Mayer, K. M.; Lee, S.; Liao, H.; Rostro, B. C.; Fuentes, A.; Scully, P. T.; Nehl, C. L.; Hafner, J. H. A Label-Free Immunoassay Based upon Localized Surface Plasmon Resonance of Gold Nanorods. *ACS Nano* **2008**, *2*, 687–692.

(36) Lin, H.-Y.; Chen, H.-A.; Lin, H.-N. Fabrication of a Single Metal Nanowire Connected with Dissimilar Metal Electrodes and Its Application to Chemical Sensing. *Anal. Chem.* **2008**, *80*, 1937–1941.

JP1014725